Chapter 2
Friction Stir Welding of Three-Dimensional Printed Polymer Composites with Semi-consumable Tool

Ranvijay Kumar, Rupinder Singh and Inderpreet Singh Ahuja

Abstract For practical applicability of friction stir welding (FSW) in repair/assembly of thermoplastics, it is required to have compatibility between two dissimilar polymers (from mechanical, morphological, chemical, and thermal view point). This study highlights that reinforcement of 15% Al powder in ABS (as ABS-15Al) and 50% to PA6 (as PA6-50Al) resulted in similar melt flow index (MFI) range of 11.57 g/10 min and 11.97 g/10, which further confirmed the enhanced material compatibility with possibility of FSW. The processing of polymer composite on twin-screw extrusion (TSE) process followed by substrate preparation on fused deposition modeling (FDM) as digital manufacturing tool has been used in the present study (to prepare functional prototypes for FSW on milling setup). The output parameters such as grain size number on stirred zone, break load, break strength, and Young's modulus of welded joints have been investigated.

Keywords Digital manufacturing · Melt flow properties · Friction stir welding · Milling

2.1 Introduction

FSW is one of the advance techniques for joining/welding of thermoplastics and thermoplastic composite materials. Some studies have reported that FSW for sheets of same materials such as high-density polyethylene (HDPE), polypropylene (PP), acrylonitrile butadiene styrene (ABS), and nylon 6 was feasible and resulted in comparable mechanical strength to the parent materials, processed with conventional experimental setups [1–4]. But at the similar condition, FSW of two dissimilar thermoplastic materials such as ABS-HDPE, poly (methyl methacrylate)

R. Kumar · R. Singh (✉)
Department of Production Engineering, Guru Nanak Dev Engineering College, Ludhiana 141006, India
e-mail: rupindersingh78@yahoo.com

I. S. Ahuja
Department of Mechanical Engineering, Punjabi University, Patiala 147 002, India

M. S. Shunmugam and M. Kanthababu (eds.), *Advances in Additive Manufacturing and Joining*, Lecture Notes on Multidisciplinary Industrial Engineering,
https://doi.org/10.1007/978-981-32-9433-2_2

(PMMA)-PMMA/silica, HDPE-Al alloy, ABS-PMMA, and HDPE-PP required the strong materials attentions such as material flow, heat generations, controlled melting during process, and optimum machining inputs [5–9]. Performing welding of two dissimilar polymeric materials requires special attentions because of differences in the material properties such as glass transition temperature, melting point, molecular weight, and carbon chain structure. Some studies suggested that silica nanocomposite reinforced PMMA sheets proposed elastic particle–particle interaction between the polymeric sheets when welded by friction spot welding [10]. The volumetric flow generally generates on thermo-mechanical heat affect zone which is the main criteria for determining final quality of the welds. Those pores can be controlled by controlling thermal degradation of the materials during processing phase [11]. Controlled heat generation mechanism can be achieved by shoulder design. It was observed in Al alloy sheet joining that heat produced on the top of the AA6082T6 sheets has soften the thermoplastic material which later provided the back-extrusion through the pre-drilled hole to assure the joining [12]. FSW for PMMA sheets has resulted in an interesting fact that during welding of metals, both shoulder and pin driven the material volume in thermo-mechanical heat-affected zone, whereas in case of polymers, only pin drives the material volume in thermo-mechanical heat-affected zone [13]. Heating the plastic material during the FSW process may be one of the alternative property improvement techniques which can make robust product. A 3-mm-thick polyethylene (PE) sample was driven by heated step pin tool, resulted in the improved welding product as prospect of mechanical strength [14]. Mechanical sustainability of the joints is highly dominated by the role of tool geometry and configuration. The FSW conducted for polypropylene and PE, the optimum pin geometry, resulted in the tensile strength 98% to the polyethylene as well as elongation and hardness greater than the base material [9]. Some researchers highlighted that mechanical, thermal, rheological, morphological, and thermo-chemical properties of the weld are largely affected by design of shoulder and pin, so for performing successful FSW operations, one should have proper design of shoulder and pin [15–18]. As most of the studies have been focused on similar material joining, but dissimilar material need to be made compatible for possible joining/welding application. Three-dimensional printers have revolutionized the digital manufacturing of functional as well as non-functional prototypes made up from polymer composites for high-precision, defect-less parts (which fits from mechanical, morphological, tribological, chemical, and thermal aspects) [4–7]. In the present study, processing of polymer composite on TSE followed by substrate preparation on FDM as digital manufacturing tool has been used (to prepare functional prototypes for FSW on milling setup). The output parameters such as grain size number (on stirred zone), break load, break strength, and Young's modulus of joint prepared have also been investigated.

2.2 Experimentation

Initially, pilot experiments were conducted for FSW (at 1200 rpm, 30 mm/min with pin diameter 7 mm) of 3D printed ABS and PA6 sheets result in weak joint (visual observations) which were failed by applying very small quantity of load. From this pilot test, it has been ascertained that ABS and PA6 are from two different class of polymers with poor welding/joining compatibility and needs some reinforcement (may be metallic/nonmetallic) material for successful welding/joining.

2.2.1 Materials and Methods

As per reported literature, ABS and PA6 have dissimilar material properties based upon their mechanical, chemical, metallurgical, and thermal behavior [6, 7]. These thermoplastic materials have significant difference in their MFI (g/10 min), specific heat capacity, chemical resistivity, melting point, and mechanical strength. The mechanical, rheological, and thermal properties of extruded filaments of virgin ABS and virgin PA6 polymers (selected for present study) are shown in Table 2.1.

FSW with the use of the semi-consumable tool (Al reinforced PA6) of shoulderless design has been selected for the present study to join sheets of substrate (Al reinforced ABS). The present method with the use of semi-consumable tool has numerous applications for repair/maintenance of cracks generated in the polymeric pipelines (see Fig. 2.1).

Table 2.1 Properties of virgin ABS and PA6 filament

Materials	MFI (g/10 min)	Melting point (°C)	Break load (N)	Break strength (MPa)	Young's modulus (MPa)
ABS	8.78	201.14	59.21	23.4	55.30
PA6	23.29	219.32	203.1	94.9	35.41

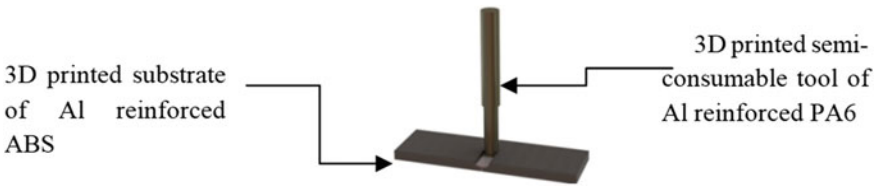

Fig. 2.1 Proposed FSW for joining 3D printed parts

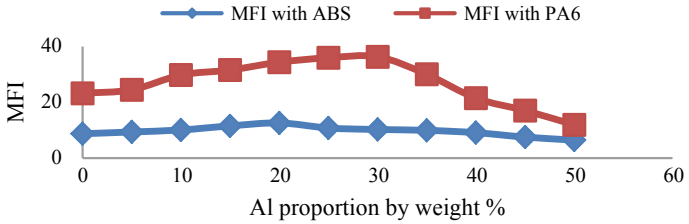

Fig. 2.2 MFI characterization of ABS and PA6 with Al powder

2.2.2 MFI

During pilot experimentation, it has been observed that joining of ABS and PA6 resulted in weak joints (may be because of dissimilar flow properties, as MFI of ABS is 8.78 g/10 min and PA6 having 23.29/10 min). Based upon those observations, a set of experiments have been conducted to evaluate the MFI of Al powder reinforced ABS and PA6. It was observed that ABS and PA6 matrix resulted in similar MFI as reinforcing 15% Al powder to ABS matrix (ABS-15Al) (11.57 g/10 min) and 50% Al powder to PA6 matrix (PA6-50AL) (11.97 g/10 min) (see Fig. 2.2).

2.2.3 DSC Analysis

The differential scanning calorimeter (DSC) under 50 mL/min N_2 gas flow with heating and cooling rate of 10 °C/min in two repeated cycles have been conducted for ABS, PA6, ABS-15Al and PA6-50Al. The first cycle of heating and cooling has been neglected with prospect of re-moving thermal history of samples, and second cycles have been considered to be the final results. It was observed that ABS-15Al and PA6-50Al came under the similar range of melting points as 201.12 and 219.35 °C, respectively (Fig. 2.3). It can be ascertained that by making MFI in a particular range, one can maintain similar melting range (as observed in the present case).

2.2.4 TSE

TSE process with the intermeshing with co-rotating twin screws has been used to prepare the feedstock filaments of 1.75 ± 0.05 mm diameter for FDM 3D printer. As per the dimensional accuracy achieved for feedstock filaments by pilot experimentation of Al reinforced polymers, the input process variables has been selected as rotational speed (rpm), applied load (Kg), and extrusion temperature (°C). For ABS-15Al, extrusion temperature of 220 °C, 30 rpm, and 20 kg load and, for PA6-50Al, extrusion temperature of 245 °C, 20 rpm, and 15 kg applied load have been selected.

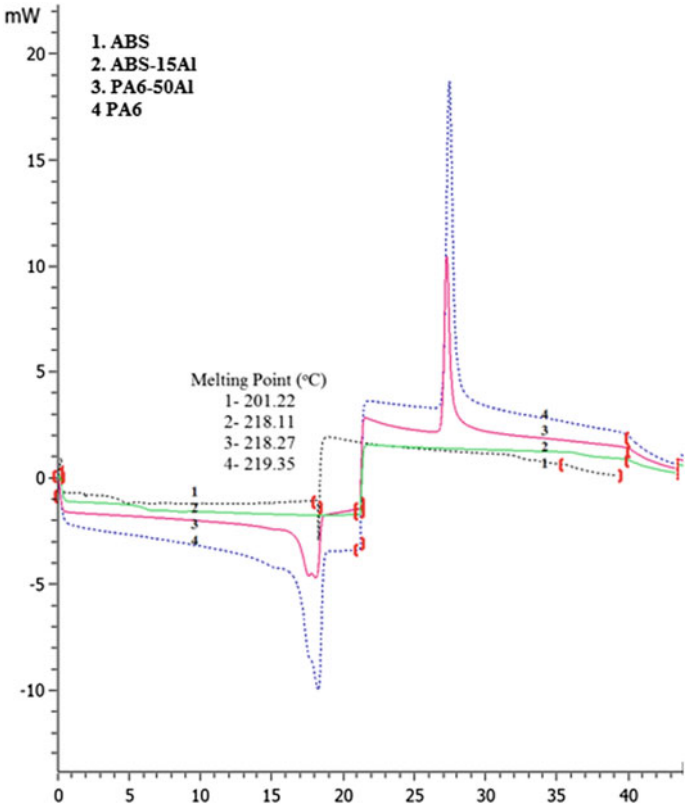

Fig. 2.3 DSC results of ABS, ABS-15Al, PA6, and PA6-50Al

2.2.5 FDM (3D Printing)

The .STL files of 3D geometry (dimensions: 50 × 30 × 3 mm) on the solid works were prepared and loaded to the processing unit of FDM for part printing. The settings of FDM printer were fixed as follows: infill density of 0.8, 06 number of perimeter, deposition angle of 60o, nozzle diameter of 0.3 mm, filament diameter of 1.75 mm, honeycomb fill pattern, perimeter speed of 30 mm/s, infill speed of 60 mm/s, travel speed of 130 mm/s, extruder temperature of 250 °C, and bed temperature of 55 °C. Rectangular sheets were prepared with ABS-15Al, whereas PA6-50Al was used to fabricate the pin profile under these same processing conditions (see Fig. 2.4).

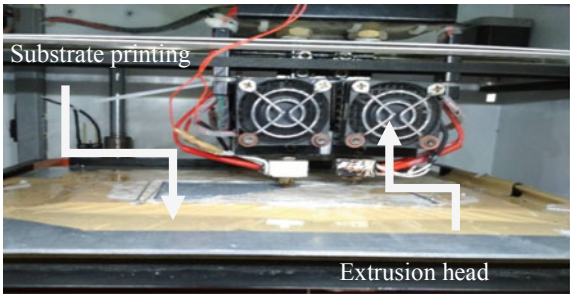

Fig. 2.4 3D printing of parts by FDM process

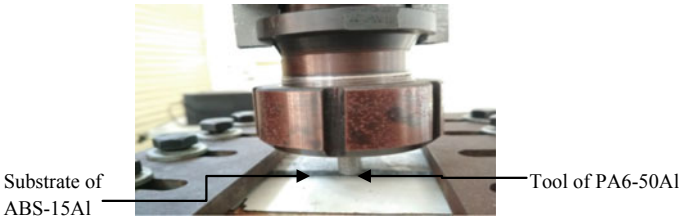

Fig. 2.5 Experimental view of FSW process

2.2.6 FSW Process

The FSW process with use of a 3D printed shoulder-less consumable pin of PA6-50Al was put to join the sheets of ABS-15Al. A vertical milling setup integrated with automated control of rotational speed and transverse speed has been selected. Figure 2.5 shows the 3D view of FSW setup.

Considering the design of experimentations based upon Taguchi L9 orthogonal array, a set of experimentation has been taken for final study of FSW as shown in Table 2.2 by considering the input process variables as rotational speed (rpm), transverse speed (mm/min), and pin diameter in mm.

2.3 Results and Discussion

It has been observed that FSW of ABS-15Al by using semi-consumable tool of PA6-50Al resulted in sound welding joints. Ultimate tensile machine (UTM) with ASTM D638 has been used to evaluate the joints' characteristics such as break load, break strength, and Young's modulus, whereas ASTM E2015-04 (2014) has been used to evaluate the microstructural grain size number at stirred zone. The evaluated properties of joints are shown in Table 2.3.

Table 2.2 Design matrix

S. No.	Rotational speed (rpm)	Transverse speed (mm/min)	Diameter of pin (mm)
1	1000	30	7
2	1000	40	8
3	1000	50	9
4	1200	30	8
5	1200	40	9
6	1200	50	7
7	1400	30	9
8	1400	40	7
9	1400	50	8

Table 2.3 Mechanical properties of the joints

Exp. No.	Break load (N)	Break strength (MPa)	Young's modulus (MPa)	Grain size number on stirred zone
1	3.07	2.55	3.79	3.50
2	6.82	5.71	6.93	3.75
3	2.26	1.88	2.45	3.50
4	9.31	7.59	19.74	1.50
5	11.17	9.31	20.01	1.75
6	8.17	6.81	18.77	3.00
7	4.49	3.65	9.27	1.25
8	7.33	6.11	10.39	1.75
9	3.90	3.18	6.32	1.75

Signal-to-noise ratio (SNR) determines the accuracy and effect of input variables of the process. SNR of the properties can be desired 'smaller is better' or 'larger is better' depending upon nature of the properties. For the properties desired 'larger is better,' SNR can be expressed as follows:

$$\eta = -10 \log \left[\frac{1}{n} \sum_{k=1}^{n} \frac{1}{y^2} \right]$$

For properties which desired 'smaller is better,' SN ratios can be calculated as follows:

$$\eta = -10 \log \left[\frac{1}{n} \sum_{k=1}^{n} y^2 \right]$$

where η is SN ratio, n is the number of experiment, and y is the material properties at experiment no. k. Based upon Table 2.3, SNR of break load, break strength, Young's modulus (selected for larger is better case), and grain size number at stirred zone (selected for smaller is better case) have been calculated (see Table 2.4).

As per calculations made to evaluate SNR for different mechanical and metallurgical properties, the main effect plots for all the properties have been drawn with help of Minitab software to see contributing input variables. Figure 2.6a–d shows the linear model for SNR of different properties (a: break load, b: break strength, c: Young's modulus, and d: grain size number on stirred zone). It has been observed that 1200 rpm, 40 mm/min transverse speed, and 8 mm pin diameter are the best settings for mechanical properties (break load, break strength, and grain size number at stirred zone), whereas 1400 rpm, 30 mm/min transverse speed, and 9 mm pin diameter are the best settings for change in grain size number at stirred zone (see Fig. 2.6). Further based upon Table 2.3, ANOVA was performed for all mechanical properties. For break load, ANOVA resulted in P value of 0.048 for input parameter as rotational speed. This means the rotational speed is the significant factor under 95% confidence limits. Transverse speed is the second most desired input parameter and pin diameter contributed least (see Table 2.5) for changes in SNR of break load. Based upon Table 2.5, response ranking has been made (see Table 2.6), which highlights that rotational speed was ranked 1, transverse speed was ranked 2, and pin diameter was ranked 3 for changes in the SNR of break load.

The optimum value of the break load can be predicted from the given Eq. (1). The optimum value can be predicted from combination of input variables suggested in Fig. 2.6 (for break load as 1200 rpm, 40 mm/min transverse speed, and 8 mm pin diameter).

$$\eta\text{opt} = m + (mA2 - m) + (mB2 - m) + (mC2 - m) \tag{1}$$

Table 2.4 SNR of evaluated properties

Exp No.	SNR (break load)	SNR (break strength)	SNR (Young's modulus)	SNR (grain size number on stirred zone)
1	9.74	8.13	11.57	−10.88
2	16.67	15.13	16.81	−11.48
3	7.08	5.48	7.78	−10.88
4	19.37	17.60	25.90	−3.52
5	20.96	19.37	26.02	−4.86
6	18.24	16.66	25.46	−9.54
7	13.04	11.24	19.34	−1.93
8	17.30	15.72	20.33	−4.86
9	11.82	10.04	16.01	−4.86

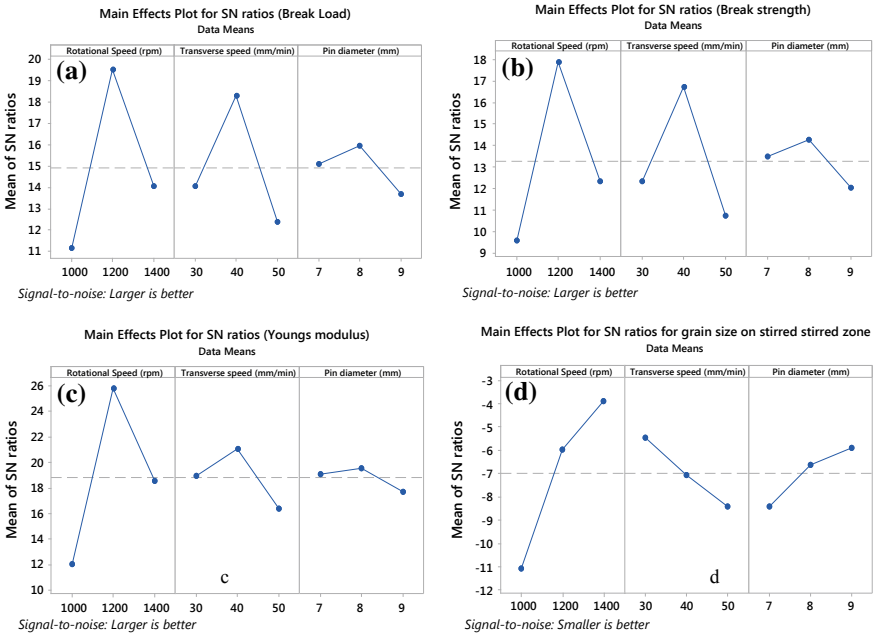

Fig. 2.6 Linear model of SNR for joints' properties

Table 2.5 ANOVA for SN ratios for break load

Source	DF	Seq SS	Adj SS	Adj MS	F	P
Rotational speed (rpm)	2	108.20	108.20	54.1	19.96	0.048
Transverse speed (mm/min)	2	56.09	56.09	28.04	10.35	0.088
Pin diameter (mm)	2	7.82	7.82	3.912	1.44	0.409
Residual error	2	5.42	5.42	2.71		
Total	8	177.53				

Table 2.6 Response table for signal-to-noise ratios (larger is better) for break load

Level	Rotational speed (rpm)	Transverse speed (mm/min)	Pin diameter (mm)
1	11.17	14.06	15.10
2	19.53	18.31	15.96
3	14.06	12.38	13.70
Delta	8.36	5.93	2.26
Rank	1	2	3

where 'm' is the overall mean of SN ratio, $mA2$ is the mean of SN ratio for rotational speed at level 2 (1200 rpm), $mB2$ is the mean of SN ratio for transverse speed at level 2 (40 mm/min), and $mC2$is the mean of SN data for pin diameter at level 2 (8 mm).

If the desired output properties are of 'maximum is better' nature (e.g., break load, break strength, young's modulus), then

$$y\text{opt2} = (1/10)\eta\text{opt}/10 \tag{2}$$

If the desired output properties are of 'minimum is better' nature (e.g., porosity, grain size number, residual stress), then

$$y\text{opt2} = (10)\eta\text{opt}/10 \tag{3}$$

From here, calculations can be made as follows: Overall mean of SN ratio (m) is the average of the SNR provided in Table 2.4.

$m = 14.92$ dB (See Table 2.4). From the response (Table 2.5), it is given as $mA2 = 19.53$, $mB2 = 18.31$, $mC2 = 15.96$. Considering the Eq. (2),

$\eta\text{opt} = 14.92 + (19.53 - 14.92) + (18.31 - 14.92) + (15.96 - 14.92)$ $\eta\text{opt} = 23.96$ dB

Inserting the value of ηopt in Eq. (3),

$y\text{opt2} = (10)\eta\text{opt}/10$

$y\text{opt2} = (10)24.90/10$

$y\text{opt} = 15.77$ N

The predicted optimum value for break load = 15.77 N. It is predicted from here that by considering the parametric combination of 1200 rpm rotational speed, 40 mm/min transverse speed, and 8 mm pin diameter, the break load value will be 15.77 N. The confirmatory experimentation has been performed on the desired setting, and it resulted in break load of 15.56 N. Similarly, for break strength, Young's modulus, and grain size number on stirred zone, the values at optimum setting have been evaluated and experimentation were performed to get actual values (see Table 2.7).

Here, it should be noted that maximum value of break load, break strength, and Young's modulus is obtained at experiment no. 5 and minimum at experiment no. 3 (see Table 2.3). A set of load vs. deflection curves have been merged for all the nine experiments, and it is denoted that maximum values of load achieved for experiment no. 5 and minimum for experiment no. 3 (see Fig. 2.7).

Table 2.7 Predicted versus actual value of properties under suggested setup

Properties	Break load (N)	Break strength (MPa)	Young's modulus (MPa)	Grain size number on stirred zone
Predicted/actual	15.77/15.56	13.09/13.21	27.67/27.25	1.15/1.0

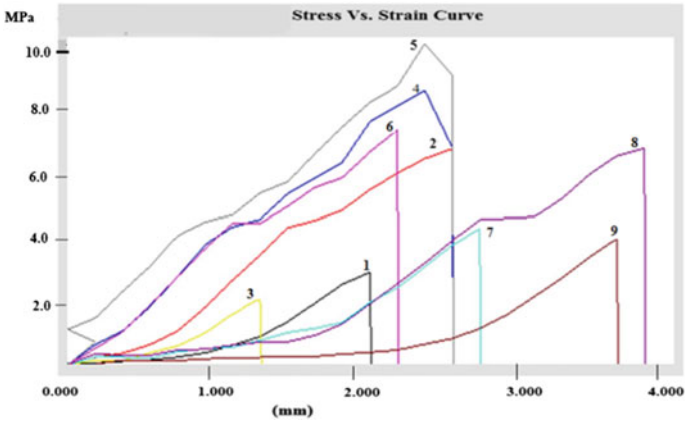

Fig. 2.7 Load versus deflection curves of welded pieces by tensile failure

The photomicrographs (under 100× magnification) obtained for experiment no. 5 and experiment no. 3 clearly show the mixing and distribution on stirred zones (see Fig. 2.8). The joints at experiment no. 3 observed as less stirred with more defective surface as compared to experiment no. 5. The proper mixing at experiment no. 5 in stirred zone strongly confirms the attainment of larger strength as compared to welded piece at experiment no. 3.

SNR for all output parameters as per Table 2.4 has been maximized for multifactor optimization. The main effect plot for SNR of combined properties suggested that 1200 rpm rotational speed; 40 mm/min transverse speed; and 8 mm pin diameter are the best settings to get the optimum properties (see Fig. 2.9).

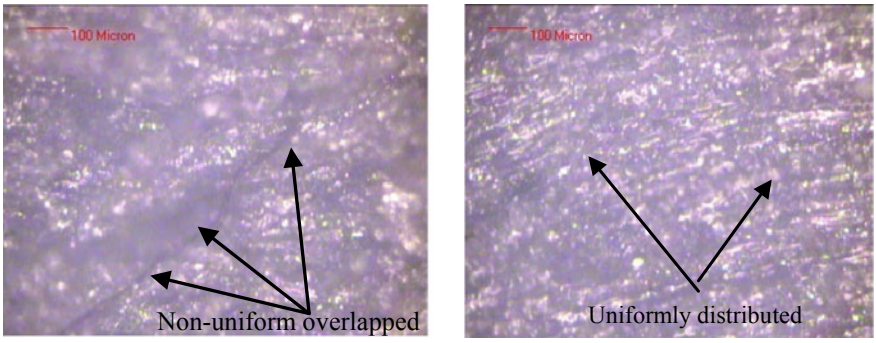

Fig. 2.8 Photomicrographs of welded joints on stirred region

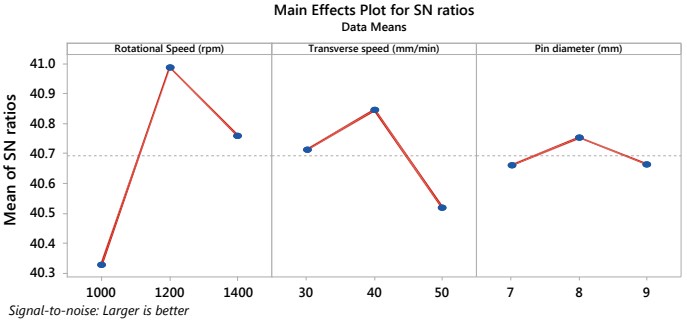

Fig. 2.9 Best settings of input parameters for multifactor optimization

2.4 Conclusions

The joining of 3D printed two virgin ABS sheets by using 3D printed virgin PA6 pin resulted in weak joints. Hence, it is strongly recommended to establish the similar properties (mechanical/thermal/rheological, etc.) of two dissimilar polymers for welding/joining applications. The deposition of PA6 material as filler was not observed.

Reinforcement of Al metal powder to ABS matrix at 15% by weight and 50% by weight in PA6 matrix resulted in the similar MFI of 11.57 g/10 min and 11.97 g/10 min. FSW performed on 3D printed parts of such polymeric composite (based upon similar MFI) resulted in the feasible welding and consumption of tool material (as filler) was observed.

Optimization of input process variable suggested that mechanical properties (break load, break strength, and Young's modulus) would be better at 1200 rpm, 40 mm/min transverse speed, and 8 mm pin diameter, whereas grain size number would be achieved minimum at 1400 rpm, 30 mm/min transverse speed, and 9 mm pin diameter.

At optimized setting of input variable, it was observed that joints sustained break strength of 56.45% to virgin ABS and 13.91% to virgin PA6. Young's modulus of joints observed 49.28% to ABS, whereas 77.21% to PA6.

Acknowledgements The authors are highly thankful to BRNS No: 34/14/10/2016-BRNS/34036 for providing financial assistance.

References

1. Panneerselvam, K., Lenin, K.: Joining of nylon 6 plate by friction stir welding process using threaded pin profile. Mater. Des. **53**, 302–307 (2014)
2. Azarsa, E., Mostafapour, A.: Experimental investigation on flexural behavior of friction stir welded high density polyethylene sheets. J. Manuf. Process. **16**(1), 149–155 (2014)

3. Sadeghian, N., Givi, M.K.B.: Experimental optimization of the mechanical properties of friction stir welded Acrylonitrile Butadiene Styrene sheets. Mater. Des. **67**, 145–153 (2015)
4. Kumar, R., Singh, R., Ahuja, I.P.S., Penna, R., Feo, L.: Weldability of thermoplastic materials for friction stir welding-a state of art review and future applications. Compos. Part B: Eng. **137**, 1–15 (2017)
5. Kumar, R., Singh, R., Ahuja, I.P.S., Amendola, A., Penna, R.: Friction welding for the manufacturing of PA6 and ABS structures reinforced with Fe particles. Compos. B Eng. **132**, 244–257 (2018)
6. Kumar, R., Singh, R., Ahuja, I.P.S.: Investigations of mechanical, thermal and morphological properties of FDM fabricated parts for friction welding applications. Measurement **120**, 11–20 (2018)
7. Singh, R., Kumar, R., Feo, L., Fraternali, F.: Friction welding of dissimilar plastic/polymer materials with metal powder reinforcement for engineering applications. Compos. B Eng. **101**, 77–86 (2016)
8. Liu, Z.Y., Xiao, B.L., Wang, W.G., Ma, Z.Y.: Singly dispersed carbon nanotube/aluminum composites fabricated by powder metallurgy combined with friction stir processing. Carbon **50**(5), 1843–1852 (2012)
9. Hajideh, M.R., Farahani, M., Alavi, S.A.D., Ramezani, N.M.: Investigation on the effects of tool geometry on the microstructure and the mechanical properties of dissimilar friction stir welded polyethylene and polypropylene sheets. J. Manuf. Process. **26**, 269–279 (2017)
10. Junior, W.S., Emmler, T., Abetz, C., Handge, U.A., dos Santos, J.F., Amancio-Filho, S.T., Abetz, V.: Friction spot welding of PMMA with PMMA/silica and PMMA/silica-g-PMMA nanocomposites functionalized via ATRP. Polymer **55**(20), 5146–5159 (2014)
11. Abibe, A.B., Sônego, M., Dos Santos, J.F., Canto, L.B., Amancio-Filho, S.T.: On the feasibility of a friction-based staking joining method for polymer–metal hybrid structures. Mater. Des. **92**, 632–642 (2016)
12. Buffa, G., Baffari, D., Campanella, D., Fratini, L.: An innovative friction stir welding based technique to produce dissimilar light alloys to thermoplastic matrix composite joints. Proced. Manuf. **5**, 319–331 (2016)
13. Simões, F., Rodrigues, D.M.: Material flow and thermo-mechanical conditions during friction stir welding of polymers: literature review, experimental results and empirical analysis. Mater. Des. **59**, 344–351 (2014)
14. Squeo, E.A., Bruno, G., Guglielmotti, A., Quadrini, F.: Friction stir welding of polyethylene sheets. Anna. Dunarea de Jos University of Galati, Technol. Mach. Build. **5**, 241–246 (2009)
15. Arora, A., De, A., DebRoy, T.: Toward optimum friction stir welding tool shoulder diameter. Scripta Mater. **64**, 9–12 (2011)
16. Rai, R., De, A., Bhadeshia, H.K.D.H., DebRoy, T.: Friction stir welding tools. Sci. Technol. Weld. Joining **16**(4), 325–342 (2011)
17. Eslami, S., Ramos, T., Tavares, P.J., Moreira, P.M.G.P.: Shoulder design developments for FSW lap joints of dissimilar polymers. J. Manuf. Process. **20**, 15–23 (2015)
18. Mendes, N., Neto, P., Loureiro, A., Moreira, A.P.: Machines and control systems for friction stir welding: a review. Mater. Des. **90**, 256–265 (2016)